# Properties of mid-latitude ice cloud from surface Ka-band radar observations during 2014-2017

Juan Huo, Yufang Tian, Xue Wu, Congzheng Han, Bo Liu, Yongheng Bi, Shu Duan and Daren Lu

Key Laboratory for Atmosphere and Global Environment Observation, Chinese Academy of Sciences

*Correspondence to*: Juan Huo (huojuan@iap.ac.cn)

**Abstract.** The physical properties and radiative role of ice clouds remain one of the uncertainties in the Earth–atmosphere system. In this study, we present a detailed analysis of ice cloud properties based on four years of surface millimetre wavelength radar measurements in Beijing, China, where summer monsoon from the ocean and winter monsoon from the continent prevails alternately, resulting in various cirrus clouds. More than 6300 ice cloud clusters were studied to quantify the properties of ice clouds, such as the height, optical depth and horizontal extent, which can serve as a reference for parameterization and characterization in global climate models. In addition, comparison between ice cloud clusters formed under summer monsoon and winter monsoon indicates the different formation and evolution mechanisms of cirrus. Statistically, the temperature of more than 95% of ice bins are below −15ºC. The dependence of the radar reflectivity of ice particles on the height and temperature was also observed in this study, indicating that the reflectivity of ice bins increases (decreases) as the temperature (height) increases. In addition, it was found that there is a strong linear relationship between the mean reflectivity and the ice cloud depth. Due to various synoptic circumstances, the ice clouds in summer are warmer, higher, and thicker, with larger reflectivity than that in winter; in particular, the mean cloud-top height of ice clouds in summer is 2.1 km higher than that in winter. It was found that cirrus clouds in winter and autumn illustrated different origin type with that in summer and spring.

## 1. Introduction

The radiative role of ice clouds in the Earth–atmosphere system is known to be significant, however, its uncertainties remain in respect of the net effects and magnitude. Cirrus clouds, composed of ice crystals, is ice cloud. Ice clouds absorb the outgoing infrared radiation from Earth's surface and lower atmosphere while reflecting a portion of the incident sunlight back to outer space. When ice clouds are thin enough that the sun can be seen through them, the net impact on the planetary radiation balance is generally one of warming; thicker ice clouds reflect more sunlight and generally result in net cooling (Heymsfield et al. 2017; Kärcher 2018; Kox et al. 2014). Ice clouds exert potential warming effects on the Earth–atmosphere energy system. Studies show that the occurrence frequency of the cirrus clouds, part of ice clouds, exhibits latitudinal variability ranging from 50% in the equatorial regions of Africa to 7% in the polar regions (Hahn and Warren 2007; Sassen et al. 2008, 2009; Stubenrauch et al.

2006). Ice clouds are an important component of the planetary radiation budget in terms of magnitude; plus, they influence hydrological and climate sensitivities and affect surface climate (Lawson et al. 2019; Yang et al. 2015).

The physical and optical properties of ice clouds, such as ice crystal size, ice shape, particle concentration, cloud-top height, and optical depth, are heterogeneously and diversely distributed over the globe (Adhikari et al. 2012; Cotton et al. 2013; Ge et al. 2019; Heymsfield et al. 2013; Jensen et al. 1996; Luebke et al. 2016; Mace et al. 2006; Yang and Fu 2009). Recent studies show that cirrus clouds remain one of the largest uncertainty sources in global climate models (GCMs), due to the deficiencies in representing their observed spatial and temporal variability (Joos et al. 2014; Muhlbauer et al. 2014; Zelinka et al. 2012). According to the IPCC (Boucher et al. 2013), "Especially for ice clouds, and for interactions between aerosols and clouds, our understanding of the basic micro-scale physics is not yet adequate, although it is improving." Understanding the microphysical and macrophysical properties of ice clouds, as well as their relationships with atmospheric states, such as temperature, wind velocity and relative humidity, is important for advancing our fundamental understanding of the formation and life cycles of ice cloud. It is also an essential step toward reducing the uncertainties of estimates of the climatic impact of cirrus and improving the representation of ice clouds in GCMs.

Millimetre wavelength radar is a powerful method for observing the macroscopic and microphysical properties of cloud vertical profiles owing to its ability to penetrate the interior of clouds. Because of their short wavelengths, they are sensitive to small cloud droplets and ice crystals, meaning they detect all types of non-precipitating clouds well (Kollias et al. 2007). Radar can perform long continuous observations and the data has high temporal resolution, which is more advantageous than the aircraft in understanding the characteristics of daily changes, the formation and development of clouds. Regular calibration for radar can ensure the stability of data and support long-term data for cloud climatology research. This study used long-term continuous surface Ka-band radar data to study and understand the microphysical and macrophysical properties of ice clouds over Beijing, China, in the northern mid-latitude region. Beijing (39.96°N, 116.37°E) is in the subtropical monsoon zone with a typical continental monsoon climate. Winds from southeast ocean prevail in summer while winds from northwest continent dominate in winter, resulting in hot and rainy summers but cold and dry winters. The formation, evolution and life cycle of ice clouds present regional and distinctive traits, which are created by the regional climate and, to a certain extent, the global climate too. This paper presents the features of ice clouds over mid-latitude monsoon regions through detailed analysis based on long-term radar data, and serves as a reference for cloud parameterization in GCMs.

Section 2 of this paper briefly introduces the Ka-band radar data, the identification method for ice clouds, and other auxiliary datasets. Section 3 describes the macrophysical properties of ice clouds. Details of the microphysical properties of ice clouds are presented in section 4. In section 5, the formation types of cirrus in four seasons are investigated. Conclusions are given in section 6.

## 2. Cirrus observation and identification by Ka-band radar

### 2.1 Ka-band radar

The ice clouds analysed in this study are from observations of a Ka-band polarization Doppler radar (KPDR) situated at the Institute of Atmospheric Physics (IAP, 39.967°N, 116.367°E), Beijing, China. KPDR was set up in 2010 and works at a frequency of 35.075 GHz (wavelength of 8.55 mm) (Huo et al. 2019), measuring the equivalent reflectivity factor ($Z_e$, hereinafter just reflectivity; units: $mm^6/m^3$; $dBZ=10\log(Z_e)$), Doppler velocity, spectral width and linear depolarization ratio of cloud. It is equipped with a Magnetron-type transmitter having a threshold of −45 dBZ for cloud determination. For a contrast, the 94 GHz cloud profiling radar (CPR) on CloudSat has a sensitivity of approximately -30 dBZ. Calculations or measurements of radar reflectivity in previous studies revealed that the reflectivity of ice clouds over mid-latitude region were mostly larger than -30 dBZ (Deng et al. 2010; Matrosov and Heymsfield 2017; Pokharel and Vali 2011). Thus, this KPDR has strong detection capability for ice clouds. The pulse width is 0.2 μs and the beam width is 0.4°. Its repetition frequency is 3.5 KHz and its vertical resolution is 30 m. KPDR has operated daily since 2012, mostly in the vertically pointing mode. During special events—for example, short-term collaborative observations with other instruments—the scanning mode changes to the Plane Position Indicator or Radar Height Indicator mode. In 2013 and 2018, KPDR was non-operational during almost the whole of the summer period. The radar data used in this paper were observed from 1 January 2014 to 31 September 2017. During these four years, the valid operational time of the radar in the vertically pointing mode occupied more than 80% of the total time. It should be noted that KPDR is more sensitive to larger particles in the cloud particle size distribution since the reflectivity is proportional to the $D^6$ (D is particle size).

### 2.2. Ice cloud identification

Cirrus is ice cloud. The Glossary of the American Meteorological Society (AMS, 2019) describes and defines cirrus cloud primarily from its appearance. However, such a definition is not applicable for the cloud classification of the KPDR data, especially those observed with a small field of few (FOV) in the vertically pointing mode. In the cloud classification algorithm developed for the CPR onboard the CloudSat satellite, the average temperature at the largest radar equivalent reflectivity factor, the average largest *Z*e, the average height of the maximum *Z*e, the cloud-base height, etc., are combined to determine cirrus cloud (Wang and Sassen 2001b). Sassen et al. (2008) classified cloud layers as cirrus via defining two criteria; namely, the visible optical depth should be less than 3.0 and the cloud-top temperature should be lower than –40 °C, categorizing cirrus clouds via cloud physical and optical parameters. Deng et al. (2010) identified cirrus layer by cloud-top and cloud-base temperature ($T_{top}$ < -40 ºC and $T_{base}$ < -10 ºC). In the studies of Krämer et al. (2016) and Luebke et al. (2016), cirrus clouds are defined as ice clouds in the temperature range < -38 ºC. Ge et al. (2019) used two temperature criteria to identify cirrus cloud: the temperature of the cloud top should be less than −30°C and the temperature at the maximum *Z*e layer and at the cloud base should be less than 0°C. Although these studies used different definition standards to identify cirrus, these clouds can be regarded as ice clouds.

KPDR has a cloud clustering and classification algorithm, a detailed description of which has been presented by Huo et al. (2019). Here, we briefly describe it as follows. The KPDR cloud profiles firstly are grouped as clusters based on a combination of a time–height clustering method and a *k*-means clustering method. After each cloud cluster is determined, a fuzzy logic method is applied using multiple cloud properties, such as cloud-base height, cloud depth, radar reflectivity, etc., to classify the cloud cluster into nine types: Cs, Cc, Ac, As, St, Sc, Ns, Cu and Cb clouds. In this study, clouds identified as Cs and Cc by KPDR are chosen for analysis. Based on the results from previous studies (Deng et al. 2010; Ge et al. 2019; Heymsfield et al. 2017; Krämer et al. 2016), in order to ensure all ice clouds are determined exactly, two criteria have been added after the classification algorithm; namely, the cloud-top temperature should be less than −40°C and the cloud-base temperature should be less than -10°C.

### 2.3 Other datasets

In this study, we also used some other datasets to complement our investigation of the properties of cirrus cloud, such as the temperature profile, water vapor, wind velocity, cloud optical thickness, etc. The research datasets of cloud optical thickness (produced from Himawari-8) used in this paper were supplied by the P-Tree System, Japan Aerospace Exploration Agency (https://www.eorc.jaxa.jp/ptree/index.html, last access: 6 January 2020). Other meteorological reanalysis data employed were from the European Centre for Medium-Range Weather Forecasts (ECMWF) ERA5 datasets (https://www.ecmwf.int/en/forecasts/datasets/reanalysis-datasets/era5; last access: 6 January 2020).

## 3. Macrophysical properties of ice clouds

### 3.1 Ice cloud samples under summer and winter monsoon

Ice clouds can be vertically and horizontally extensive, with their various appearances dependent on the diverse range of associated atmospheric movements and processes. KPDR is located in the north of the North China Plain, where to the west and north are mountains and to the south and east is the Bohai Sea. In the region's hot summers, monsoon from the sea brings large quantities of water vapor, whereas dry and cold monsoon from the northern continent dominates this region in winter. These different monsoon types support various atmospheric conditions, such as increasing relative humidity, cooling, updrafts, etc., required for the formation of ice clouds, ultimately resulting in distinct cirrus distributions. Figure 1 presents a typical example of an ice cloud distribution collected by KPDR in one month of winter (January 2016) and one month of summer (August 2015).

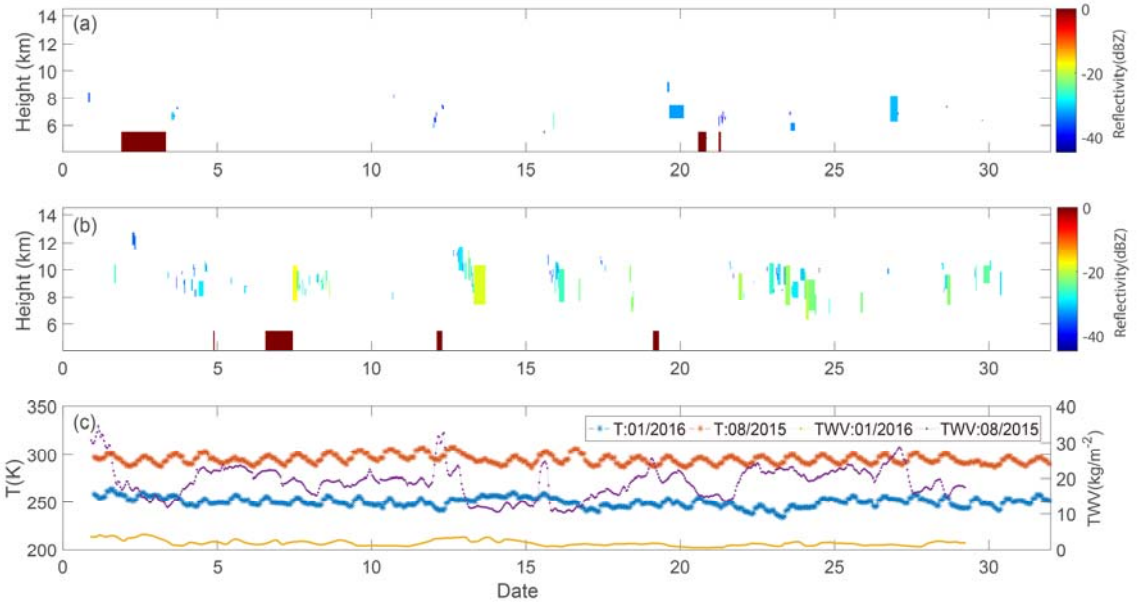


**Figure 1.** Ice clouds occurring in (a) January 2016 (winter) and (b) August 2015 (summer). The mean cloud-top height, mean base height and lifetime of each ice cluster forms an ice cloud "rectangle". Its mean radar reflectivity is illustrated with different colours. Dark red rectangles on the horizontal axis indicate periods without vertically pointing radar measurements. The surface temperature (T, left-hand *y*-axis) and total water vapor (TWV, right-hand *y*-axis) in the two months are presented in (c).

There are more ice clouds in August than in January, and the mean radar reflectivity of ice cloud in August is higher than that in January. Ice clouds in August also show larger vertical dimensions than in January. The temperature and amount of water vapor are two key parameters in the formation of clouds, especially in plain areas where orographic uplift is negligible. The strong contrast in the climatic circumstances between a month in summer and a month in winter generates a diverse range of ice clouds (Fig. 1c). Thus, to better understand the physical or optical properties of ice clouds, statistical analyses were carried out in this study for different seasons. Such comparisons of the ice clouds among the four seasons benefit our understanding of the dominant formation origins of ice clouds when a region is governed alternately by different monsoon types. In this study, four years of radar observations presented more than 6300 ice cloud clusters for our analysis.

### 3.2 Monthly and hourly occurrence frequency of ice clouds

Radar data collected in vertically viewing mode were used to calculate the occurrence frequency of all clouds ($O_{all}$), which is the ratio of cloudy profiles to all profiles in a certain time range (i.e., an hour or a month), as well as the occurrence frequency of ice clouds ($O_{ic}$), which is the ratio of profiles containing ice to all radar profiles:

$$O_{all} = N_{all} / N_r, \quad (1)$$

$$O_{ic} = N_{ic} / N_r, \quad (2)$$

where $N_{all}$ is the number of cloudy profiles, $N_r$ is the number of all radar profiles, and $N_{ic}$ is the number of ice clouds profiles. Figure 2 shows the monthly occurrence frequency of all clouds and ice clouds in four years. In addition, the occurrence frequency of cirrus clouds (picked out from ice clouds by cloud-base temperature < -38ºC) is also presented for a contrast. September has the maximum $O_{all}$ among all months, and summer/winter has the maximum/minimum $O_{all}$ among the four seasons. Relative to $O_{all}$, $O_{ic}$ decreases to 1/2–1/3, and in winter $O_{ic}$ is about 33% of $O_{all}$. The average $O_{ic}$ in April and June is about 20%, whereas in winter (December–February) it is no more than 10%. The average $O_{ic}$ in the four years is 14%, which is lower than the ice cloud coverage of 24% reported by Hahn and Warren (2007) based on satellite measurements over North China. This might be associated with the observation location and the FOV of the KPDR. Large quantities of water vapor over the sea areas and orographic-lift movements over mountain areas provide advantageous conditions for the formation of clouds, meaning more clouds occur over these areas relative to plain areas. Therefore, the occurrence frequency calculated from the KPDR data with a small FOV are lower than the cloud coverage calculated from data with a broad FOV. For cirrus clouds, the largest occurrence frequency (4%) occurs in April. Spring but not summer has the most cirrus clouds.

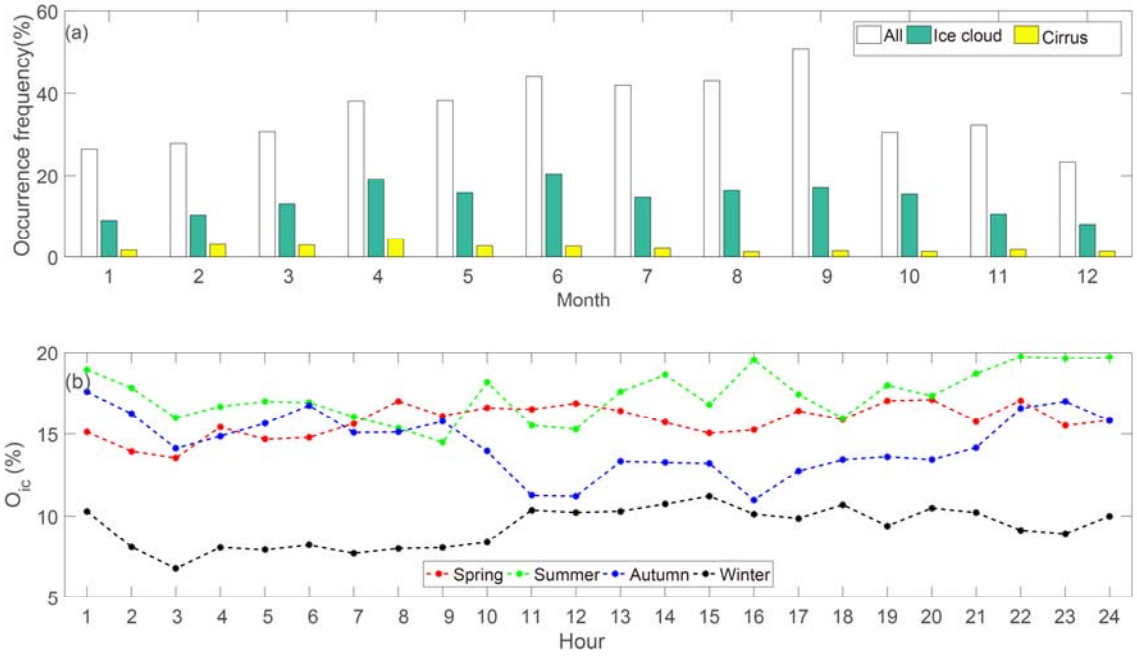


**Figure 2.** Monthly occurrence frequencies of all clouds ($O_{all}$), ice clouds ($O_{ic}$) and cirrus clouds (a) along with the diurnal $O_{ic}$ in the four seasons (b).

KPDR operates continuously and thus allows the diurnal variation of $O_{ic}$ to be studied, which illustrates the potential relationship with local thermal convection caused by solar heating. As shown in Fig. 2a, the three highest $O_{ic}$ values in spring, summer, autumn and winter occur at 20:00/22:00/19:00, 21:00/23:00/22:00, 00:00/22:00/21:00 and 14:00/13:00/17:00, respectively. The hourly variations of $O_{ic}$ in four seasons are different; in spring, summer, autumn, larger $O_{ic}$ values appear at

night while larger $O_{ic}$ values in winter appear at daytime. The diurnal variation of $O_{ic}$ seems to be insensitive to solar heating, which drives the development of regional thermal convection. Here, the presence of ice clouds over KPDR is not closely related with local air-updraft activities, indicating that these ice clouds may not be generated locally by thermal convections. It is interesting that $O_{ic}$ decreases from 00:00 to 2:00 and then increase after that in four seasons. Is there an extinction process in ice clouds during this period? Further analysis are required to testify the assumption in future.

### 3.3 Height, depth and extent of ice clouds

The top height of cirrus clouds indicates the highest condensation level in the troposphere, above which clouds cannot form because of the non-conducive condensation conditions. The base height of ice clouds indicates the lowest level required for ice formation. In this study, the cloud-top height (CTH) and cloud-base height (CBH) were calculated for each ice cloud cluster; specifically, the CTH and CBH are the mean values of all cloudy profiles in an ice cloud cluster. The distributions of the mean CTH and CBH of all ice clouds in the four seasons are presented in Fig. 3, and Table 1 presents the quantified statistical results.

It is shown that the CTH of ice clouds varies in the range of 5.5–12.9 km (Fig. 3a). The difference between the maximum CTH and the minimum CTH is about 7 km in each season, indicating the ranges of the condensation level and various formation mechanisms of ice clouds. Besides, differences in the CTH between the four seasons are also apparent. Both the maximum CTH (13.35 km) and the highest mean CTH (10.16 km) are found in summer, whereas winter has the minimum CTH (11.25 km) and lowest mean CTH (7.66 km). In summer, 98% of ice clouds have a CTH greater than 8 km and 57% are greater than 10 km. In winter, only 37% of ice clouds have a CTH larger than 8 km, and those with a CTH higher than 6 km account for 94%. The mean CTH in summer is 2.5 km higher than that in winter, which means the average condensation level in summer is also 2.5 km higher. Spring and autumn are two transition seasons and their CTHs are 8.95 km and 9.09 km, respectively, which are between those of summer and winter.

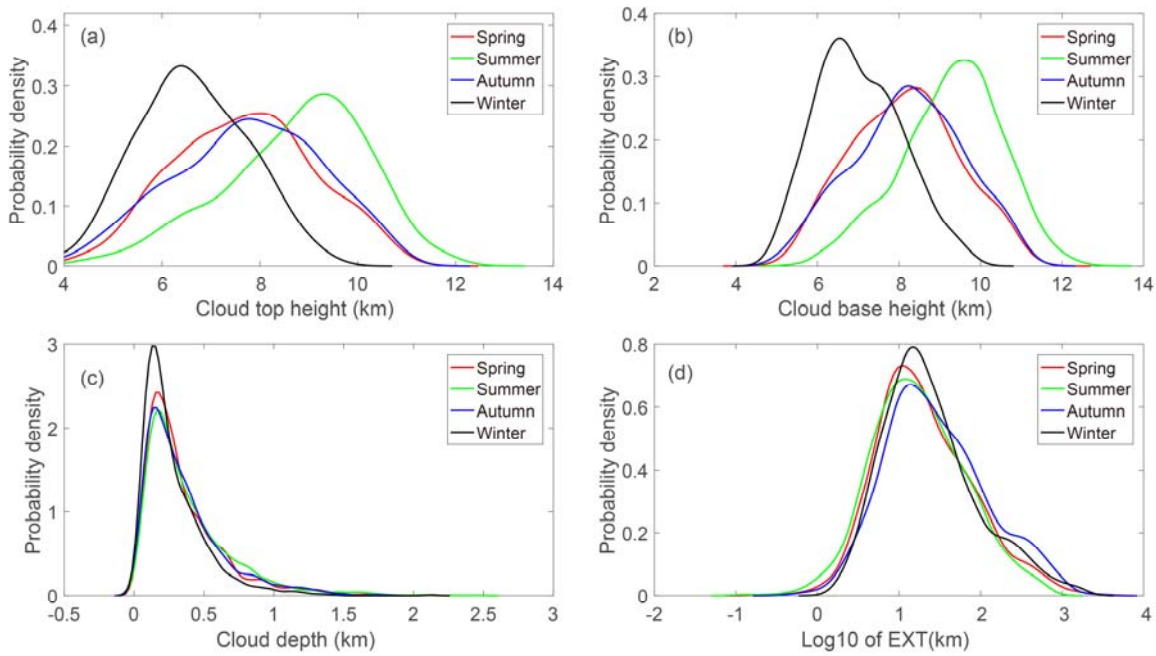


**Figure 3.** Distribution of cloud-top height (CTH) (a), cloud-base height (CBH) (b), cloud depth (CD) (c) and horizontal extent (EXT) (d) in the four seasons. In (d), EXT is shown as log10 values.

Figure 3b shows that the CBH changes within a range of 5–12.4 km, and the minimum CBHs in the four seasons are close to each other, ranging between 5.3 and 5.7 km. However, the mean CBH in summer is the highest (8.7 km) among the four seasons, while the lowest (6.6 km) is in winter. The difference in CBH between summer and winter is 2.1 km. Both mean CBHs in spring and autumn are 7.7 km. In summer, the percentage of ice clouds with a CBH larger than 8 km is 72%, while it is only 65% in winter. In winter, 71% of ice clouds have a CBH greater than 6 km.

It is shown that the mean cloud depths (CDs) of ice clouds in the four seasons are close, with the depths of most clusters being less than 1 km (Fig. 3c). Statistically, in the four seasons, 68% of clusters have a CD of less than 0.5 km, 90% less than 1 km, and 96% less than 1.5 km. It should be noted that the CTH, CBH and CD here are the mean values of an ice cloud cluster. It is therefore possible that there are some instances of CTH, CBH and CD that are greater than their corresponding mean values.

The horizontal extent (EXT) of ice clouds indicates its lifetime and the formation mechanism type. For the KPDR, the EXT of an ice cloud cluster is computed as follows:

$$\mathrm{EXT} = V_{\mathrm{hw}} \times T_{\mathrm{ci}}, \qquad (3)$$

where $V_{\mathrm{hw}}$ is the mean velocity of horizontal wind calculated from the ECMWF-ERA5 dataset and $T_{\mathrm{ci}}$ is the continuous time during which a ice cluster moves over the KPDR. It is found that the maximum EXT of ice clouds reaches 2800 km, which is in April 2017, and the maximum $T_{\mathrm{ci}}$ is 21 hours, which is in March 2016. The EXT ranges through orders of magnitude from low values of less than 0.1 km to over 2800 km. Summer has the minimum mean, median and trimmed mean EXT,

while ice clouds in autumn have the maximum mean, median and trimmed mean EXT. Statistically, about 75% of ice clouds have an EXT less than 50 km and 87% less than 100 km. The statistically quantified structural properties of ice clouds in the four seasons are presented in Table 1.

**Table 1.** Statistical results for the cloud-top height (CTH), cloud-base height (CBH), cloud depth (CD) and horizontal extent (EXT) in the four seasons. The 'trimmean' is the 10% trimmed mean of portion clusters, excluding 10% of clusters with the highest and lowest values (units: km).

| Season | Parameters | Mean | Median | Trimmean | Maximum | Minimum |
|---|---|---|---|---|---|---|
| Spring | CTH | 8.16 | 8.17 | 8.15 | 11.74 | 5.73 |
| | CBH | 7.68 | 7.68 | 7.68 | 11.43 | 5.43 |
| | CD | 0.35 | 0.27 | 0.32 | 2.1 | 0.06 |
| | EXT | 61.5 | 17.34 | 35.6 | 2824.9 | 0.18 |
| | COD | 4.27 | 3.22 | 3.81 | – | 0.06 |
| Summer | CTH | 9.27 | 9.38 | 9.30 | 12.86 | 6.10 |
| | CBH | 8.73 | 8.97 | 8.78 | 12.42 | 5.64 |
| | CD | 0.39 | 0.30 | 0.35 | 2.45 | 0.06 |
| | EXT | 43.0 | 16.1 | 29.6 | 725.1 | 0.13 |
| | COD | 6.07 | 4.28 | 5.64 | – | 0.1 |
| Autumn | CTH | 8.23 | 8.27 | 8.24 | 11.25 | 5.69 |
| | CBH | 7.74 | 7.80 | 7.77 | 11.07 | 5.31 |
| | CD | 0.35 | 0.28 | 0.33 | 1.82 | 0.06 |
| | EXT | 86.10 | 23.5 | 55.17 | 2863.8 | 0.47 |
| | COD | 4.62 | 3.05 | 4.01 | – | 0.01 |
| Winter | CTH | 7.02 | 6.90 | 7.00 | 9.94 | 5.50 |
| | CBH | 6.63 | 6.57 | 6.63 | 9.75 | 5.30 |
| | CD | 0.28 | 0.21 | 0.26 | 2.13 | 0.04 |
| | EXT | 72.7 | 19.3 | 41.4 | 1695.2 | 1.50 |
| | COD | 4.52 | 2.80 | 4.10 | – | 0.21 |

### 3.4 Optical depth of ice clouds

Cloud optical depths (COD) are relatively independent of wavelength throughout the visible spectrum. In the visible portion of the spectrum, the COD is almost entirely due to scattering by droplets or crystals of clouds (AMS, 2019). Therefore, the CODs of ice clouds depend directly on the CD, the ice water content, and the size distribution of the ice crystals, indicating a cooling effect or warming effect in the energy budget.

The Advanced Himawari Imager (AHI), onboard the geostationary meteorological Himawari-8 satellite operated by the Japanese Meteorological Agency, observes the Beijing area every 10 min and began releasing COD and cloud-type products in July 2015 with a spatial resolution of 5 km. The CODs are retrieved by using nonabsorbing visible wavelengths (i.e., 0.51

or 0.64 μm) and water-absorbing near-infrared wavelengths (i.e., 1.6 or 2.3 μm) (Kawamoto et al. 2001; Nakajima and Nakajma 1995). Quantified uncertainties of the AHI-CODs have not been reported, so we use them here directly. The data nearest to KPDR that AHI determines as cirrus cloud and KPDR determine as ice cloud type are selected and their CODs are investigated. Those collocated CODs (collected from the year 2016 to 2017) in the four seasons, combined with the mean CDs and mean reflectivity, which are calculated from all cloudy KPDR bins observed within 10 min of the AHI observing time, are presented in Fig. 4.

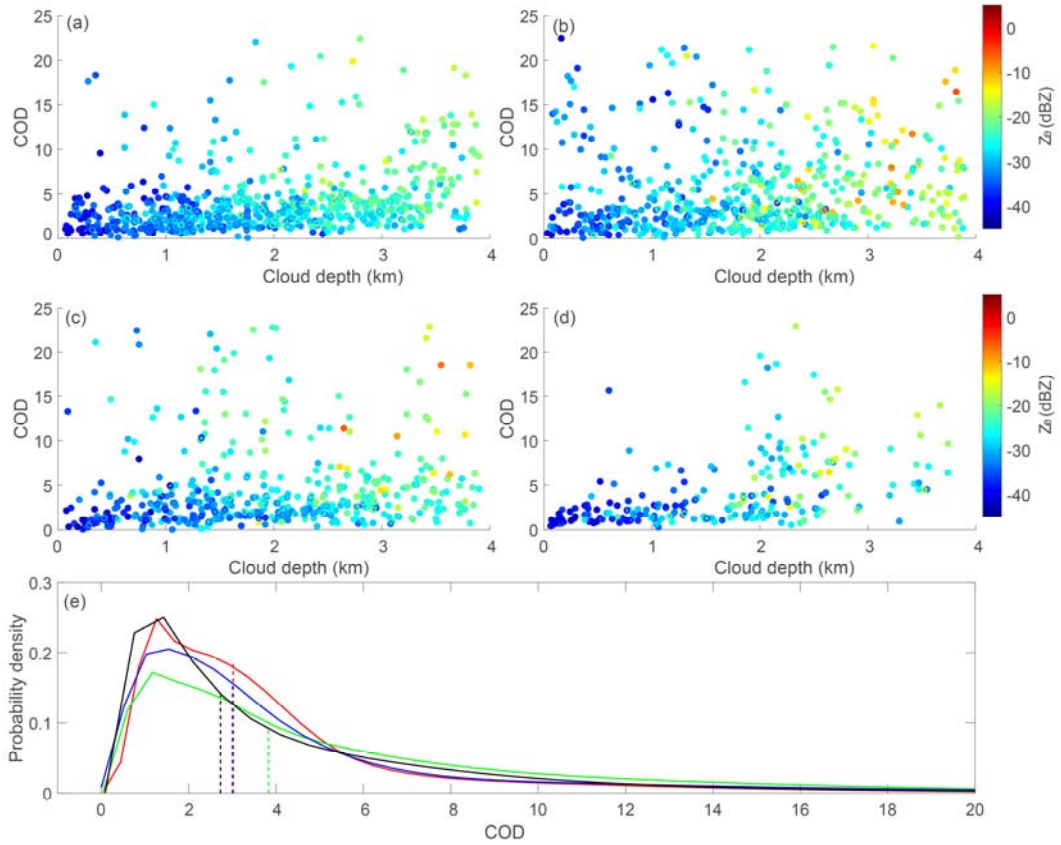


**Figure 4.** The cloud optical depth (COD) of ice clouds in terms of the cloud depth (CD) in spring (a), summer (b), autumn (c), and winter (d). Colors indicate the mean radar reflectivity of those radar profiles within 10 min of the AHI observation time. Panel (e) presents the probability density distribution of the COD in the four seasons.

In the four seasons, CODs show an increasing tendency with increasing CD. The mean reflectivity shows a similar tendency, meaning thicker ice clouds generally contain larger particles and a greater number density of ice particles. The probability density distributions of COD in the four seasons show a higher probability occurring at lower COD. The mean COD in spring, summer, autumn and winter is 4.27, 6.07, 4.62, and 4.52, respectively. The proportions of CODs lower than 3 in spring, summer, autumn and winter are 46%, 36%, 49% and 52%, respectively. The proportions of CODs lower than 10 in spring, summer, autumn and winter are 91%, 79%, 87% and 90%, respectively.

## 4. Microphysical properties of ice clouds

The most important microphysical quantities of ice clouds are the ice particle size distribution, the ice water content (IWC), and their shapes (Heymsfield et al. 2017). It is known that the radar equivalent (or effective) reflectivity factor can be expressed as

$$Z_e=\frac{\lambda^4}{\pi^5}\left|\frac{m^2-1}{m^2+2}\right|^{-2}\iiint \sigma(D,\theta,\Phi)N(D,\theta,\Phi)\mathrm{d}D\mathrm{d}\theta\mathrm{d}\Phi, \quad (4)$$

where $\sigma(D,\theta,\emptyset)$ is the backscattering cross section with maximum dimension $D$ and an axial direction $(\theta,\emptyset)$ with respect to the radar beam, $N(D,\theta,\emptyset)$ is the number density, $\lambda$ is the wavelength, and $m$ is the complex index of refraction of the scattering target. To date, numerous empirical relationships between $Z_e$ and cloud properties ($P$)—e.g., IWC, snow precipitation rate—have been developed, usually in the power-law form of

$$Z_e = AP^B, \quad (5)$$

where $A$ is the prefactor coefficient and $B$ is the exponent derived in terms of calculated or measured datasets (Austin et al. 2009; Delanoë and Hogan 2010; Deng et al. 2015; Heymsfield et al. 2018; Heymsfield et al. 2008; Liu and Illingworth 2000; Matrosov and Heymsfield 2017; Wang and Sassen 2001a). Delanoë and Hogan (2008, 2010) proposed a different method using a forward model to retrieve the IWC and the effective radius by combination with the COD. Also, the basic principles of this method are applied in the CloudSat/CALIPSO cloud microphysical retrieval algorithm. However, the utility of empirical relations such as Eq. (5) is still common in many practical measurements, and the correspondence between the IWC and $Z_e$ is related with the particle size distribution (the gamma distribution is mostly used for ice clouds).

For the KPDR, the development of the IWC and particle size retrieval algorithm is in progress but has not been tested completely. In this paper, we use the measured radar reflectivity factor $Z_e$ directly, not the retrieved microphysical quantities, to study and characterize the microphysical properties of ice clouds. It can be found from the Eq. (4) that reflectivity increases when $\sigma$ and $N$ increase; in other words, a larger reflectivity normally indicates a larger $D$, $N$ and IWC.

### 4.1 Reflectivity of ice clouds and height dependence

KPDR detects clouds at a 30-m vertical resolution. All ice radar bins collected from 2014 to 2017 were counted according to their reflectivity and height, and the relative frequencies are shown separately in Fig. 5 (calculated by 0.25 dBZ and 30 m interval). In summer, the reflectivity mostly varies between −35 and −10 dBZ, while most of the reflectivity falls within the range of −40 to −20 dBZ in winter. In spring and autumn, the reflectivity primarily ranges between −35 and −15 dBZ. The range of variation in reflectivity in summer is the biggest among the four seasons, while it is smallest in winter. Statistically, at the same height where ice clouds exist in the four seasons, the mean reflectivity of winter is 5 dBZ less than that of spring or autumn, and it is 10 dBZ less than that of summer. In the four seasons, the mean reflectivity declines as the height increases, with a similar slope. It can also be seen that the ice bins in summer are located at higher heights than in winter.

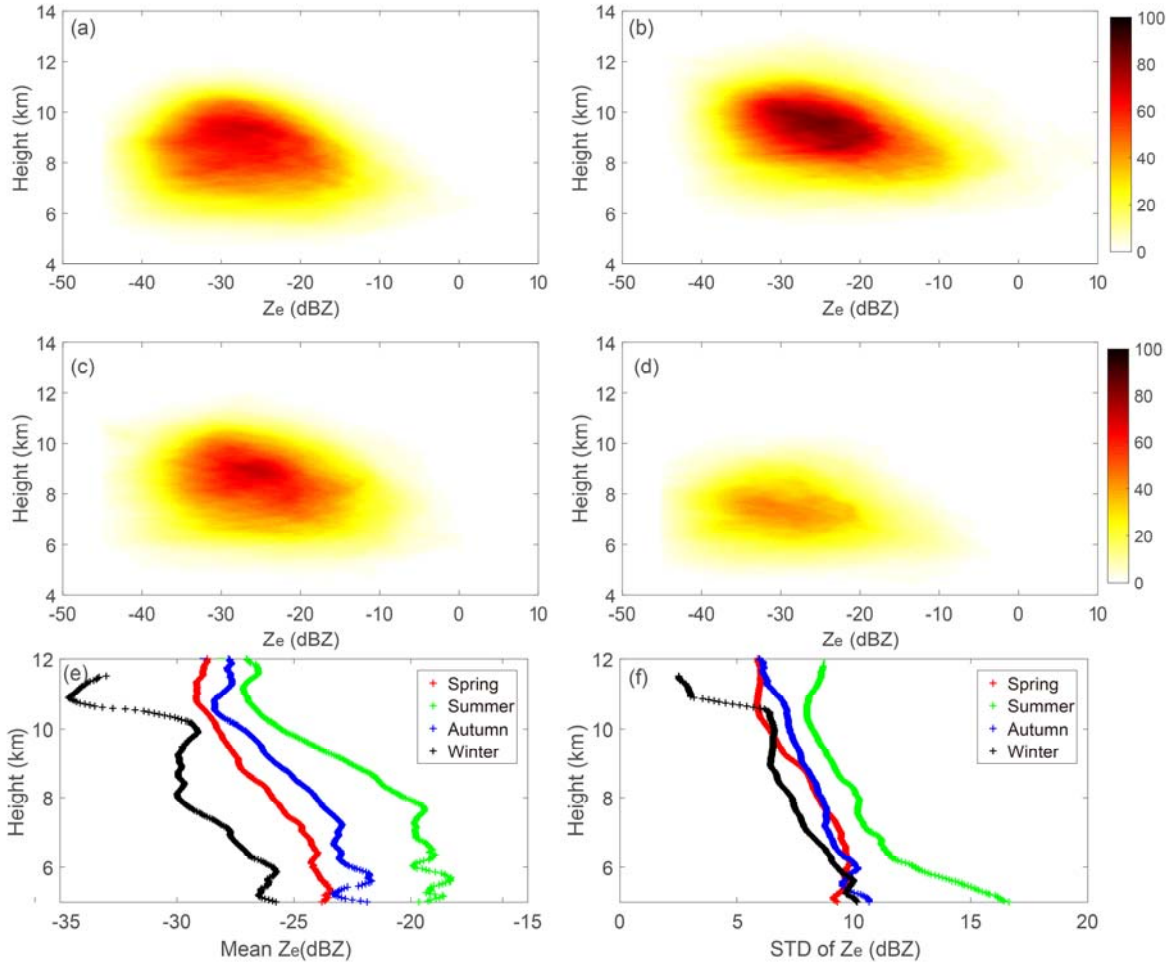


**Figure 5.** The frequency of reflectivity versus height in spring (a), summer (b), autumn (c) and winter (d). Colors are the values of the numbers divided by 1000. The mean reflectivity calculated at various heights and the corresponding standard deviation (STD) are presented in (e) and (f), respectively.

### 4.2 Temperature dependence

Temperature plays a key role in the formation, evolution and lifetime of ice clouds. Activation of liquid waterdrops does not happen below −38ºC because the relative humidity where the ice forms is below water saturation. At temperatures higher than −38ºC, ice clouds can form heterogeneously or homogeneously (Kanji et al. 2017). The summer monsoon and winter monsoon in Beijing support distinct temperatures, water vapor, etc., i.e., the conditions necessary for the formation of ice clouds, resulting in distributions of reflectivity with different features corresponding to temperature (calculated by 0.25 dBZ and 1 ºC interval, see Fig. 6).

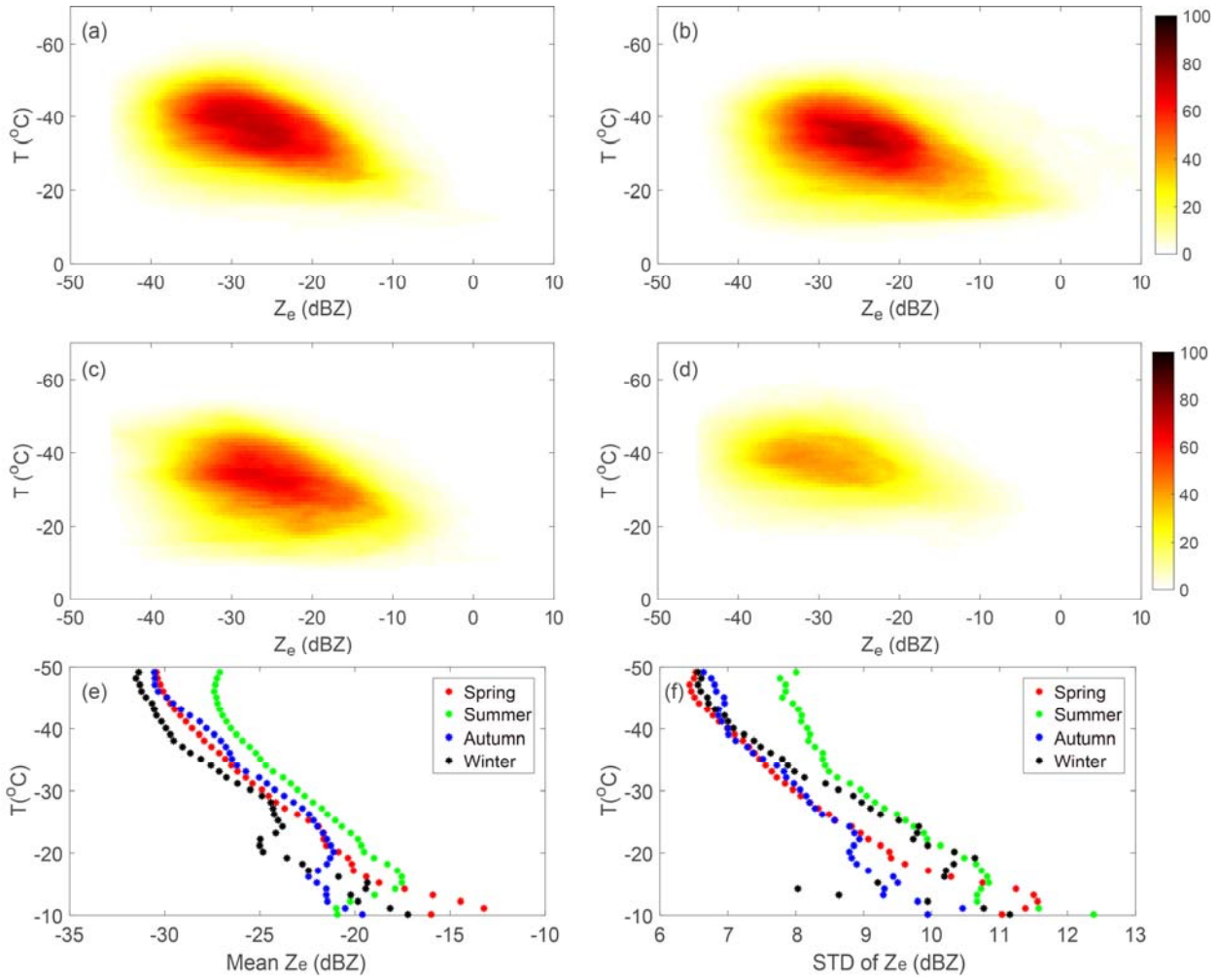


**Figure 6.** As in Fig. 5 but for temperature, and the colors are the values of the numbers divided by 5000.

In spring, summer and autumn, ice clouds occur mostly at temperatures within the range of −20ºC to −45ºC, relative to which ice clouds in winter occur at lower temperatures. Statistically, the frequency of ice bins with temperatures less than −15ºC is 99%, 95%, 95% and 99% in spring, summer, autumn and winter, respectively; the frequency of ice bins with temperatures less than −25ºC is 85%, 71%, 72% and 92% in spring, summer, autumn and winter, respectively; the frequency of ice bins with temperatures less than −35ºC is 52%, 36%, 35% and 60% in spring, summer, autumn and winter, respectively. The reflectivity shows a dependence on the temperature, increasing when temperature increases. Statistically, the mean temperature of ice clouds in winter is lower than that in other seasons, even though these ice clouds appear at lower heights. As the temperature decreases, the difference in reflectivity between winter and summer declines. At the same temperature, the mean reflectivity in summer is higher than that in winter. The slopes among four seasons are close to each other, demonstrating a determinative effect of the temperature on the cloud particle properties.

### 4.3 Depth dependence

Based on all the ice clusters in the four years, we calculated the mean reflectivity and the mean depth of each cluster (Fig. 7), and it was interesting to find that there is a strong linear relationship between the mean reflectivity and the CD. The mean reflectivity increases as the CD increases. The linear equation shown in Fig. 7 represents a method that can be used to estimate the mean reflectivity (or CD) if the CD (or reflectivity) is known, which should be useful for cloud parameterization in GCMs.

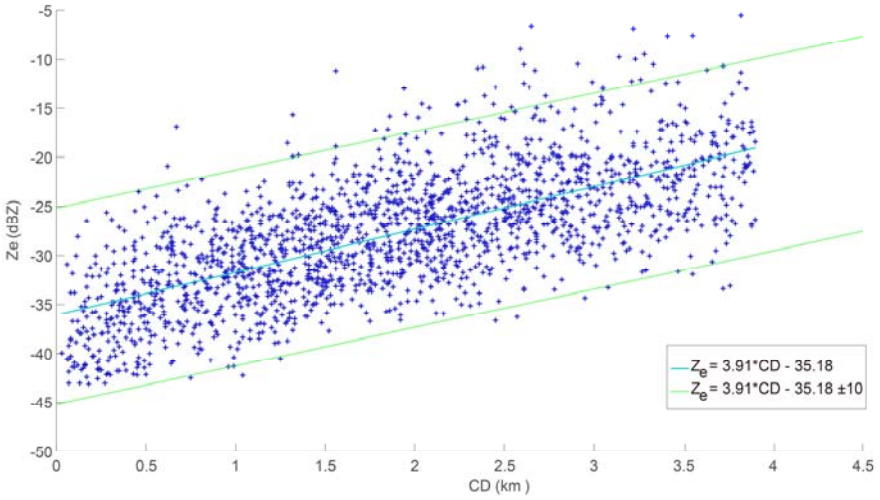


**Figure 7.** The mean reflectivity of ice clouds as a function of cloud depth (CD).

## 5. Origination type of cirrus clouds

Kramer et al (2016) and Luebke et al. (2016) classified two types of cirrus cloud according to their formation mechanism; namely, *in situ*- and liquid-origin cirrus cloud. The *in situ*-origin cirrus type forms directly as cirrus, while the liquid-origin type originates from mixed-phase clouds that are completely frozen until they are lifted to the ice formation temperature region. They reported that the *in situ*-origin cirrus are mostly thin, with lower IWC, while liquid-origin cirrus tend to be thicker with higher IWC. Also, liquid-origin cirrus tend to have larger ice crystals than *in situ*-origin cirrus. Various prefactor coefficients dependent on temperature have been derived and applied in the $Z_e$–IWC power-law relationship [i.e., Eq. (5)] since the distribution of reflectivity has a dependence on temperature, just as shown in above section 4.2 (Heymsfield et al. 2018; Heymsfield et al. 2013; Hogan et al. 2006; Matrosov and Heymsfield 2017). Therefore, the reflectivity of *in situ*-origin cirrus should generally be less than that of liquid-origin cirrus.

In this section, based on the frequency statistics in section 4.2, we calculated the distribution of reflectivity (similar to the probability density function, PDF) at several temperatures to investigate the origin type of cirrus in Beijing. Figures 8~11 show the normalized frequency of reflectivity at central temperature of −65ºC, −60ºC, −55ºC, −50ºC, −45ºC and −40ºC within ±1ºC in spring, summer, autumn and winter, respectively.

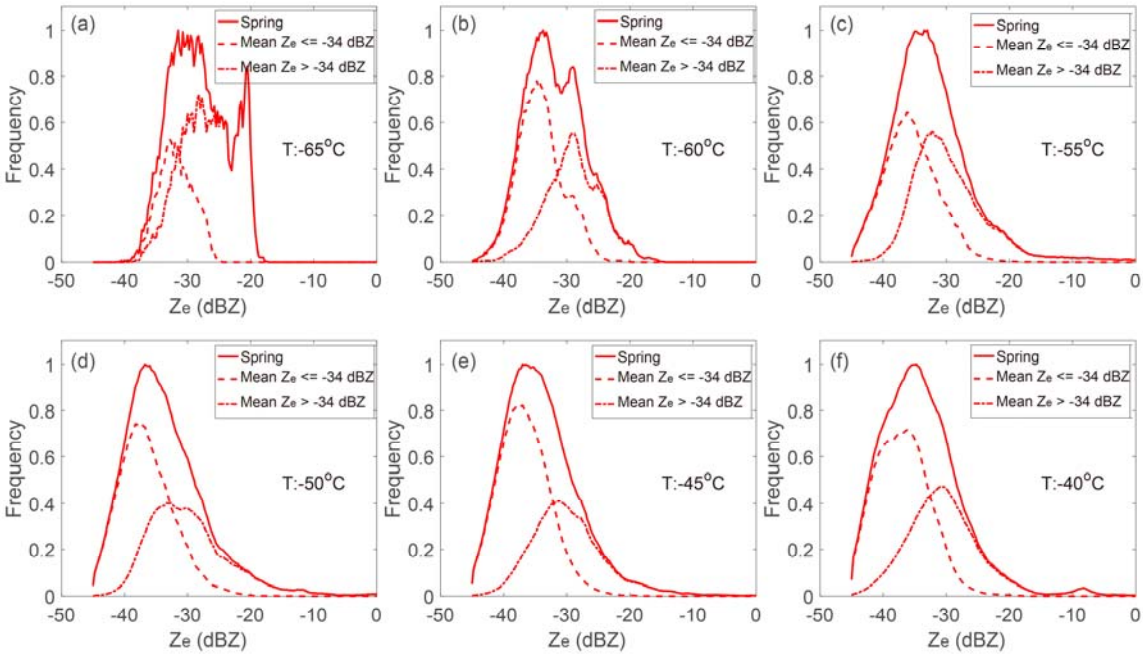


**Figure 8.** Normalized frequency of the reflectivity at different temperatures in spring. Solid line is the frequency calculated from all cirrus. Dashed line is the frequency calculated from cirrus with mean Ze less than -34 dBZ. Dash-dotted line is the frequency calculated from cirrus with mean Ze above -34 dBZ.

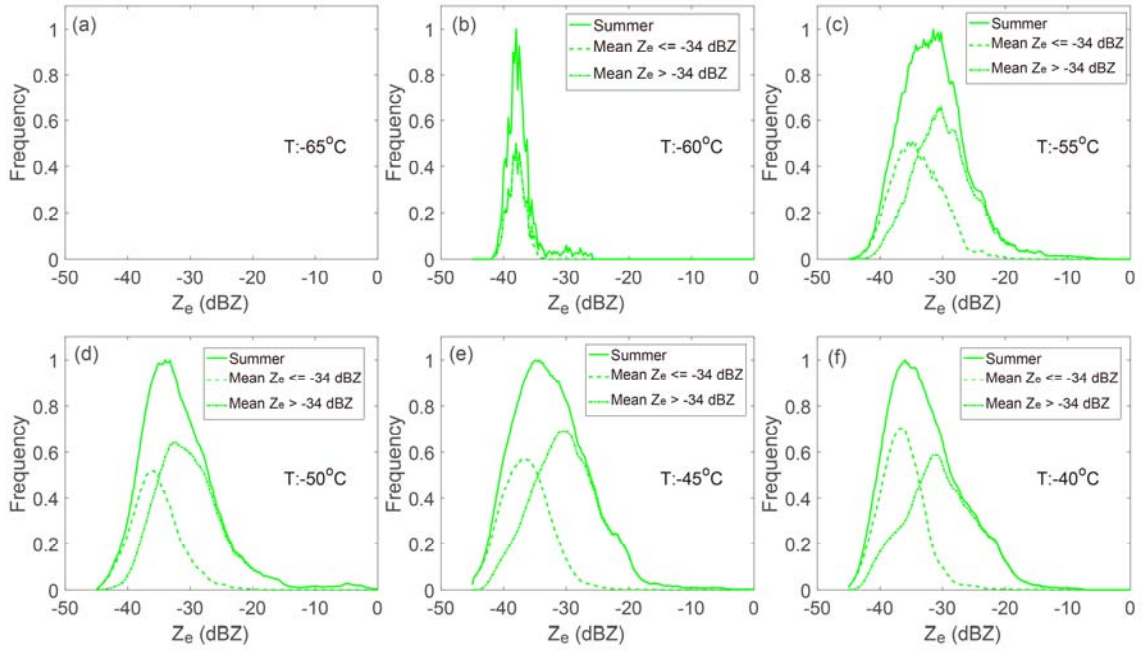


**Figure 9.** Same as Figure.8 but for summer. No cirrus is found when temperature is below -65 ºC in summer.

Cirrus clouds present diverse reflectivity frequency distributions in terms of temperature in four seasons. There is no cirrus cloud detected in summer and autumn below −65ºC. Above −55ºC, the peak frequency center in winter locates at smaller reflectivity value than that in summer. The bimodal PDF is found at some temperatures, for example the temperature at −60ºC and -65ºC in spring and at the temperature −45ºC in autumn. However, most PDFs show a unimodal feature. One possibility is that only one origin type exists in Beijing. Another possibility is that difference between the two origin types is not clearly distinguished. It might be related with the measurement specialties of radar since the Ze indicates the backscattering from numerous particles and the Ze is more sensitive to larger particles in the particle size distribution.

We divide cirrus clouds into two groups using mean-Ze threshold to study whether cirrus clouds in Beijing are also originated from different mechanisms. If the PDFs of two separate groups exhibit distinct features, it is possible that they form from different mechanisms. It is found that the cirrus clouds in spring and summer (Fig.8 and Fig.9) were separated clearly into two groups by threshold of -34 dBZ and the two groups demonstrated different PDF. The full width at half maxima and the peak center is different. In addition, the proportions of the two groups are comparable. However, in autumn and winter, cirrus clusters with mean reflectivity less than −34 dBZ contribute the absolute majority of all cirrus clusters when compared with the cirrus with reflectivity larger than −34 dBZ, illustrating different PDFs with those in spring and summer. It is possible that the differences in the PDF among four seasons is due to the different origin type. For mean Ze <= -34 dBZ, cirrus cloud is likely to be an *in situ*-origin cirrus; for mean Ze > -34 dBZ, cirrus cloud is likely to be a liquid-origin cirrus. From Fig.8 and Fig.9, it can be seen that spring has more *in situ*-origin cirrus while summer has more liquid-origin cirrus. In winter and autumn, the cirrus that mean Ze <= -34 dBZ dominates, which means that dominant cirrus in winter and autumn are *in situ*-origin cirrus.

As mentioned above, there might be another possibility that only one origin type dominates over Beijing since most PDFs are unimodal. Large-scale synoptic and dynamic analysis should be made to distinguish the dominant origin type. At present, we prefer there are two origin types in Beijing. More works will be performed in future to confirm current assumptions. On the whole, the formation mechanism of cirrus in spring and summer in Beijing illustrate different features to that in autumn and winter. It also can be found that the distribution of reflectivity depends not only on the temperature but also on the origin type.

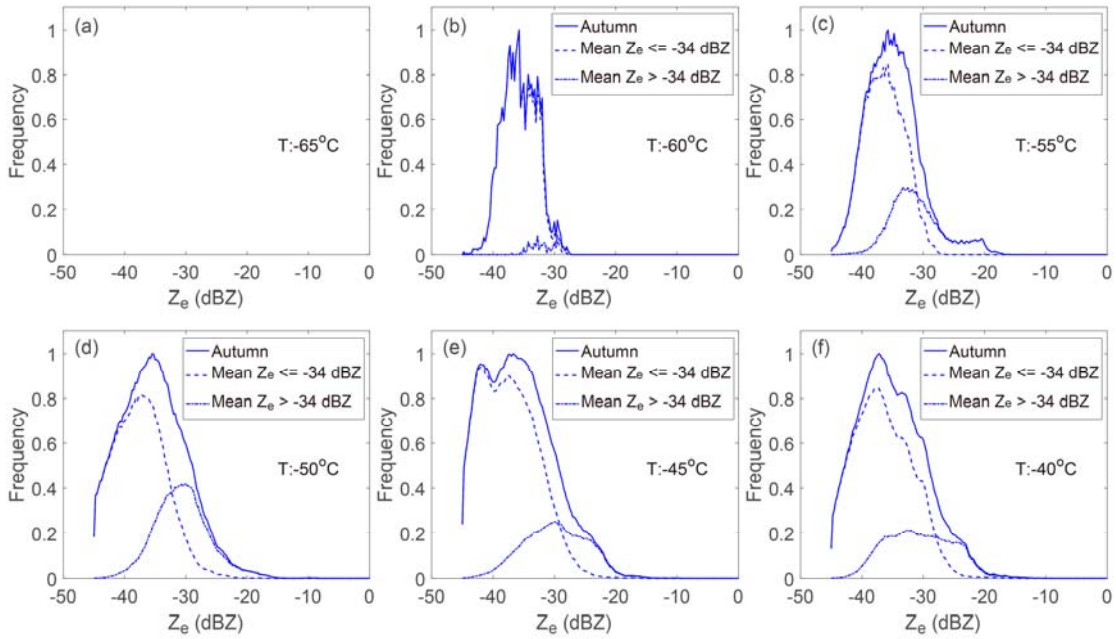


**Figure 10.** Same as Figure.8 but for autumn. No cirrus is found when temperature is below -65 ºC in autumn.

335

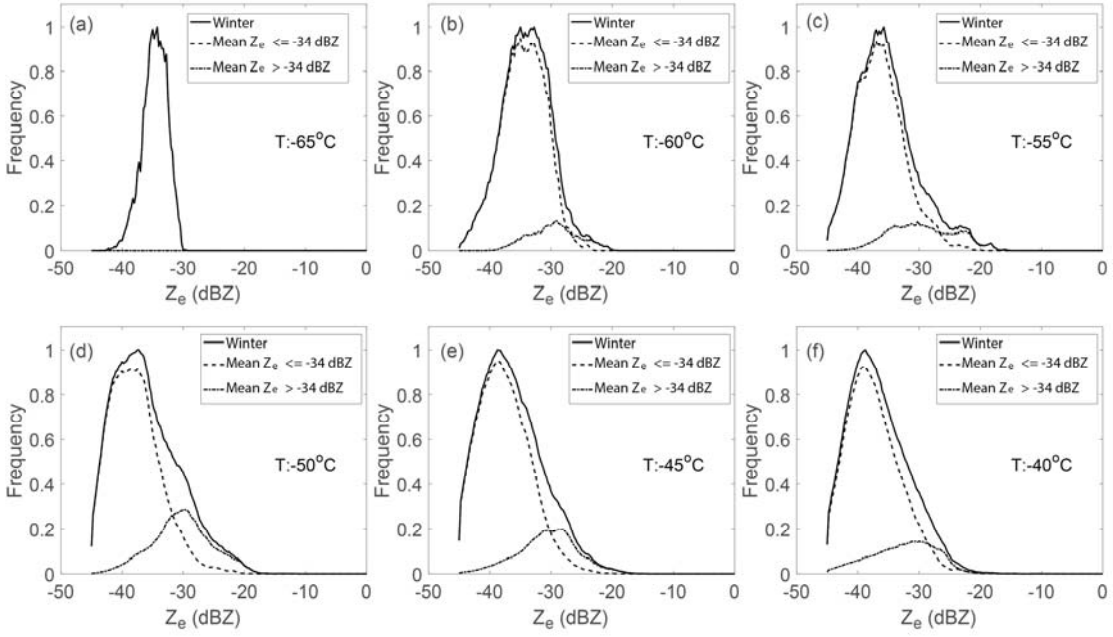


**Figure 11.** Same as Figure.8 but for winter.

## 6. Summary and discussion

Ice clouds are an important component of the planetary radiation budget and remain an uncertainty source in GCMs. This study used four years of vertically pointing Ka-band radar measurements at Beijing to characterize the physical and optical properties of ice clouds and to investigate the origination type of cirrus cloud. The goal was to present the quantified properties of ice clouds over the subtropical monsoon zone, which can be represented in GCMs towards a better understanding of the relationships between temperature and radar reflectivity under different formation conditions in various monsoon climates.

Winter monsoon and summer monsoon prevail alternately over Beijing, resulting in four distinct seasons. Ice clouds in winter and summer show strikingly different features. The specific findings about the properties of ice clouds can be summarized as follows:

1. The occurrence frequency, height, temperature and mean reflectivity of ice cloud in winter are lower than in summer. The average occurrence frequency over Beijing is 14%, and it is 20% in summer but less than 10% in winter. The diurnal variation of the occurrence frequency is not obvious, indicating an insensitive response to solar heating.
2. The CTHs of ice clouds range within 5.5–12.9 km, and the difference between the maximum and minimum reaches 6 km in every season. The mean CTH in summer is 2.5 km higher than in winter. The CBHs range within 5–12.4 km, and the difference in the mean CBH between summer and winter is 2.1 km. In total, 86% of ice clouds are above 7 km in summer, and 81% are above 7 km in winter. Statistically, in the four seasons, 68% of clusters have a depth of less than 0.5 km, 90% less than 1 km, and 96% less than 1.5 km.
3. The EXT ranges through orders of magnitude from low values of less than 0.1 km to over 2800 km. Summer has the minimum mean, median and trimmed mean EXT, whereas ice clouds in autumn have the maximum mean, median and trimmed mean EXT. Statistically, about 75% of ice clouds have an EXT less than 50 km and 87% less than 100 km. In addition, the mean COD in spring, summer, autumn and winter is 4.3, 6.1, 4.6 and 4.5, respectively.
4. The radar reflectivity of ice clouds are dependent on the height, temperature and CD. The reflectivity mostly varies between −35 and −10 dBZ, and the mean reflectivity in summer is 10 dBZ higher than in winter. More than 95% of ice bins are below the temperature of −15ºC, and the mean temperature of ice cloud in winter is the lowest among the four seasons. It was found that there is a strong linear relationship between the mean reflectivity and the CD.

The PDFs of reflectivity for cirrus cloud with respect to various temperatures were also investigated. It was found that the PDFs in four seasons illustrate striking differences. A superficial analysis indicates that cirrus clouds with mean reflectivity lower than −34 dBZ are likely to be of the *in situ*-origin type. Most cirrus clouds are of the *in situ*-origin type in winter and autumn; the *in situ*-origin type cirrus clouds are more than liquid-origin cirrus clouds in spring while summer have more liquid-origin cirrus clouds. In future work, we intend to further investigate the formation mechanisms of cirrus clouds in Beijing, as well as in other areas, for the purposes of parameterization in GCMs and the development of a locally adaptive $Z_e$–IWC relationship.

## Data Availability

The MODIS product data were obtained from http://ladsweb.nascom.nasa.gov. The AHI data were obtained from https://www.eorc.jaxa.jp/ptree/index.html. The radar data used here are available by special request to the corresponding author (huojuan@mail.iap.ac.cn).

## Author contributions

Juan Huo designed the study and carried it out. Yufang Tian, Congzheng Han, Xue Wu, Yinan Wang, Yongheng Bi and Bo Liu prepared some of the datasets. Juan Huo prepared the manuscript with contributions from all co-authors.

## Competing interests

The authors declare that they have no conflicts of interest.

## Acknowledgments

This work was supported by the National Natural Science Foundation of China (grant 41775032). We appreciate the valuable suggestions and insightful instructions from the reviewers. Thanks also to the ECMWF-ERA5 and AHI science teams for sharing their product datasets. We also acknowledge our Ka-radar team for their maintenance service during long-term measurements that made our research possible.

## References

Adhikari, L., Z. Wang and M. Deng: Seasonal variations of antarctic clouds observed by cloudsat and calipso satellites. J. Geophys. Res. Atmos., 117(doi:10.1029/2011JD016719), D04202, 2012.

American Meteorological Society, cited 2019: Ice. Glossary of Meteorology. Available online at http://glossary.ametsoc.org/wiki/ Ice.

Austin, R. T., A. J. Heymsfield and G. L. Stephens: Retrieval of ice and cloud microphysical parameters using the cloudsat millimeter-wave radar and temperature. J. Geophys. Res. Atmos., 114 doi: 10.1029/2008JD010049,2009.

Boucher, O., D. Randall, P. Artaxo, C. Bretherton and e. al: Clouds and aerosols, in climate change 2013: The physical science basis. Contribution of working group i to the fifth assessment report of the intergovernmental panel on climate change, edited by t. F. Stocker et al.,. Cambridge Univ. Press,Cambridge, U. K., and New York, 2013.

Cotton, R. J., P. R. Field, Z. Ulanowski, P. H. Kaye, E. Hirst, R. S. Greenaway, I. Crawford, J. Crosier and J. Dorsey: The effective density of small ice particles obtained from in situ aircraft observations of mid-latitude ice. Quarterly Journal of the Royal Meteorological Society, 139(676), 1923-1934, doi: 10.1002/qj.2058,2013.

Delanoë, J. and R. J. Hogan: A variational scheme for retrieving ice cloud properties from combined radar, lidar, and infrared radiometer. J. Geophys. Res. Atmos., 113(D7), doi: 10.1029/2007jd009000,2008.

Delanoë, J. and R. J. Hogan: Combined cloudsat-calipso-modis retrievals of the properties of ice clouds. J. Geophys. Res. Atmos., 115(D4), doi: 10.1029/2009jd012346,2010.

Deng, M., G. G. Mace, Z. Wang, and H. Okamoto: Tropical composition, cloud and climate coupling experiment validation for cirrus cloud profiling retrieval using CloudSat radar and CALIPSO lidar, J. Geophys. Res. Atmos., 115, D00J15, doi:10.1029/2009JD013104,2010.

Deng, M., G. G. Mace, Z. Wang and E. Berry: Cloudsat 2c-ice product update with a new ze parameterization in lidar-only region. J. Geophys. Res. Atmos., 120(23), 12,198-112,208, doi: 10.1002/2015jd023600,2015.

Ge, J., Z. Wang, Y. Liu, J. Su, C. Wang and Z. Dong: Linkages between mid-latitude ice cloud properties and large-scale meteorology at the sacol site. Climate Dynamics, 53 5035–5046, doi: https://doi.org/10.1007/s00382-019-04843-9,2019.

Hahn, C. J. and S. G. Warren (2007). A gridded climatology of clouds over land (1971–96) and ocean (1954–97) from surface observations worldwide. Numeric Data Product NDP-026E, Carbon Dioxide Information Analysis Center, Oak Ridge National Laboratory, Oak Ridge.

Heymsfield, A., A. Bansemer, N. B. Wood, G. Liu, S. Tanelli, O. O. Sy, M. Poellot and C. Liu: Toward improving ice water content and snow-rate retrievals from radars. Part ii: Results from three wavelength radar–collocated in situ measurements and cloudsat–gpm–trmm radar data. J. Appl. Meteorol. Climatol., 57(2), 365-389, doi: 10.1175/jamc-d-17-0164.1,2018.

Heymsfield, A., C. Schmitt and A. Bansemer: Ice cloud particle size distributions and pressure-dependent terminal velocities from in situ observations at temperatures from 0º to 86ºc. J. Atmos. Sci., 70 4123–4154, doi: doi:10.1175/JAS-D-12-0124.1,2013.

Heymsfield, A. J., M. Krämer, A. Luebke, P. Brown, D. J. Cziczo, C. Franklin, P. Lawson, U. Lohmann, G. McFarquhar, Z. Ulanowski and K. V. Tricht: Ice clouds. Meteorological Monographs, 58 2.1-2.26, doi: 10.1175/amsmonographs-d-16-0010.1,2017.

Heymsfield, A. J., A. Protat, D. Bouniol, R. T. Austin, R. J. Hogan, J. Delanoë, H. Okamoto, K. Sato, G.-J. v. Zadelhoff, D. P. Donovan and Z. Wang: Testing iwc retrieval methods using radar and ancillary measurements with in situ data. J. Appl. Meteorol. Climatol., 47(1), 135-163, doi: 10.1175/2007jamc1606.1,2008.

Hogan, R. J., M. P. Mittermaier and A. J. Illingworth: The retrieval of ice water content from radar reflectivity factor and temperature and its use in evaluating a mesoscale model. J. Appl. Meteorol. Climatol., 45(2), 301-317, doi: 10.1175/jam2340.1,2006.

Huo, J., Y. BI, D. Lu and S. Duan: Cloud classification and distribution of cloud types in beijing using ka band radar data. Advances in Atmospheric Sciences, 36 1-11, doi: https://doi.org/10.1007/s00376-019-8272-1.,2019.

Jensen, E. J., O. B. Toon, H. B. Selkirk, J. D. Spinhirne and M. R. Schoeberl: On the formation and persistence of subvisible ice clouds near the tropical tropopause. J. Geophys. Res. Atmos., 101(D16), 21361-21375, doi: 10.1029/95jd03575,1996.

Joos, H., P. Spichtinger, P. Reutter and F. Fusina: Influence of heterogeneous freezing on the microphysical and radiative properties of orographic ice clouds. Atmos. Chem. Phys.,, 6835–6852, doi: doi:10.5194/acp-14-6835-2014,2014.

Kanji, Z. A., L. A. Ladino, H. Wex, Y. Boose, M. Burkert-Kohn, D. J. Cziczo and M. Krämer: Overview of ice nucleating particles. Meteorological Monographs, 58 1.1-1.33, doi: 10.1175/amsmonographs-d-16-0006.1,2017.

Kärcher, B.: Formation and radiative forcing of contrail ice. Nature Communications, 9(1), 1824, doi: 10.1038/s41467-018-04068-0,2018.

Kawamoto, K., T. Nakajima and T. Y. Nakajima: A global determination of cloud microphysics with avhrr remote sensing. Journal of Climate, 14(9), 2054-2068, doi: 10.1175/1520-0442(2001)014<2054:Agdocm>2.0.Co;2,2001.

Kollias, P., E. E. Clothiaux, M. A. Miller, B. A. Albrecht, G. L. Stephens and T. P. Ackerman: Millimeter-wavelength radars: New frontier in atmospheric cloud and precipitation research. Bulletin of the American Meteorological Society, 88(10), 1608-1624, doi: 10.1175/bams-88-10-1608,2007.

Kox, S., L. Bugliaro and A. Ostler: Retrieval of ice cloud optical thickness and top altitude from geostationary remote sensing. Atmos. Meas. Tech., 7(10), 3233-3246, doi: 10.5194/amt-7-3233-2014,2014.

Krämer, M., C. Rolf, A. Luebke, A. Afchine, N. Spelten, A. Costa, J. Meyer, M. Zöger, J. Smith, R. L. Herman, B. Buchholz, V. Ebert, D. Baumgardner, S. Borrmann, M. Klingebiel and L. Avallone: A microphysics guide to ice clouds – part 1: Ice types. Atmos. Chem. Phys.,, 16 3463–3483,, doi: doi:10.5194/acp-16-3463-2016,2016.

Lawson, R. P., S. Woods, E. Jensen, E. Erfani, C. Gurganus, M. Gallagher, P. Connolly, J. Whiteway, A. J. Baran, P. May, A. Heymsfield, C. G. Schmitt, G. McFarquhar, J. Um, A. Protat, M. Bailey, S. Lance, A. Muehlbauer, J. Stith, A. Korolev, O. B. Toon and M. Krämer: A review of ice particle shapes in ice formed in situ and in anvils. J. Geophys. Res. Atmos., 124 10049–10090, doi: https://doi.org/10.1029/2018JD030122,2019.

Liu, C.-L. and A. J. Illingworth: Toward more accurate retrievals of ice water content from radar measurements of clouds. Journal of Applied Meteorology, 39(7), 1130-1146, doi: 10.1175/1520-0450(2000)039<1130:Tmaroi>2.0.Co;2,2000.

Luebke, A. E., A. Afchine, A. Costa, J. U. Grooß, J. Meyer, C. Rolf, N. Spelten, L. M. Avallone, D. Baumgardner and M. Krämer: The origin of midlatitude ice clouds and the resulting influence on their microphysical properties. Atmos. Chem. Phys., 16(9), 5793-5809, doi: 10.5194/acp-16-5793-2016,2016.

Mace, G., S. Benson and E. Vernon: Ice clouds and the large-scale atmospheric state: Relationships revealed by six years of ground-based data. J. Climate Appl. Meteor., 19 3257-3278, doi: doi:10.1175/JCLI3786.1,2006.

Matrosov, S. Y. and A. J. Heymsfield: Empirical relations between size parameters of ice hydrometeor populations and radar reflectivity. J. Appl. Meteorol. Climatol., 56(9), 2479-2488, doi: 10.1175/jamc-d-17-0076.1,2017.

Muhlbauer, A., T. P. Ackerman, J. M. Comstock, G. S. Diskin, S. M. Evans, R. P. Lawson and R. T. Marchand: Impact of large-scale dynamics on the microphysical properties of midlatitude ice. J. Geophys. Res. Atmos., 119 3976–3996, doi: doi:10.1002/2013JD020035,2014.

Nakajima, T. Y. and T. Nakajma: Wide-area determination of cloud microphysical properties from noaa avhrr measurements for fire and astex regions. Journal of the Atmospheric Sciences, 52(23), 4043-4059, doi:

10.1175/1520-0469(1995)052<4043:Wadocm>2.0.Co;2,1995.

Pokharel, B. and G. Vali: Evaluation of collocated measurements of radar reflectivity and particle sizes in ice clouds: J. Appl. Meteorol. Climatol., 50, 2104-2119, 2011.

Sassen, K., Z. Wang and D. Liu: Global distribution of ice clouds from cloudsat/cloud-aerosol lidar and infrared pathfinder satellite observations (calipso) measurements. J. Geophys. Res., 113(D00A12), doi: doi:10.1029/2008JD009972,2008.

Sassen, K., Z. Wang and D. Liu: Ice clouds and deep convection in the tropics: Insights from calipso and cloudsat. J. Geophys. Res. Atmos., 114, doi: D00H06, doi:10.1029/2009JD011916,2009.

Stubenrauch, C. J., A. Chedin, G. Radel, N. A. Scott and S. Serrar: Cloud properties and their seasonal and diurnal variability from tovs path-b. J. Clim., 19(21), 5531–5553, 2006.

Wang, Z. and K. Sassen: Ice cloud microphysical property retrieval using lidar and radar measurements. Part i: Algorithm description and comparison with in situ data. Journal of Applied Meteorology, 41 218-229, 2001a.

Wang, Z. and K. Sassen: Cloud type and macrophysical property retrieval using multiple remote sensors. Journal of Applied Meteorology, 40(10), 1665-1682, doi: 10.1175/1520-0450(2001)040<1665:Ctampr>2.0.Co;2,2001b.

Wolf, V., T. Kuhn, M. Milz, P. Voelger, M. Krämer and C. Rolf: Arctic ice clouds over northern sweden: Microphysical properties studied with the balloon-borne ice cloud particle imager b-ici. Atmos. Chem. Phys., 18(23), 17371-17386, doi: 10.5194/acp-18-17371-2018,2018.

Yang, P., K. N. Liou, L. Bi, C. Liu, B. Yi and B. A. Baum: On the radiative properties of ice clouds: Light scattering, remote sensing, and radiation parameterization. Adv. Atmos. Sci.,, 32 doi: https://doi.org/10.1007/s00376-014-0011-z,2015.

Yang, P. and Q. Fu: Dependence of ice crystal optical properties on particle aspect ratio. Journal of Quantitative Spectroscopy and Radiative Transfer, 110(14–16), 1604-1614, doi: https://doi.org/10.1016/j.jqsrt.2009.03.004,2009.

Zelinka, M. D., S. A. Klein and D. L. Hartmann: Computing and partitioning cloud feedbacks using cloud property histograms. Part i: Cloud radiative kernels. J. Clim., 25(11), 3715–3735, 2012.